

Development of HELIOS/BIPR/PARCS/MCNP6 computation route for WWER RPV neutron fluence analysis and validation against ex-vessel detectors measurement data

S. Bznuni* , A. Ugujyan, A. Amirjanyan

*Nuclear and Radiation Safety Center,
4 Tigran Mets, 0010, Yerevan Armenia*

P. Kohut

*Brookhaven National Laboratory,
33 North Renaissance Road, Upton, NY 11973*

E-mail: s.bznuni@nrsc.am

List of the total number of pages

1. Cover Page – 1 page
2. Abstract – 1 page
3. Manuscript text (including embedded figures and references) – 12 pages

Development of HELIOS/BIPR/PARCS/MCNP computation route for WWER RPV neutron fluence analysis and validation against ex-vessel detectors measurement data

S. Bznuni*, A. Ugujyan, A. Amirjanyan, P. Kohut

Abstract – A computational route was developed for the precise calculation of the fast neutron fluence on the WWER type reactor pressure vessel (RPV). The method is based on the transfer of neutronics data from HELIOS-2 lattice calculations, nodal diffusion neutronics data (power, density, temperature) from BIPR7.1 and PARCS 3.36/PATHS core calculations into 3D (pin-wise axially distributed) fixed neutron source for modeling of transport of fast neutrons from reactor core to the outer surface of RPV using MCNP6.2.

Validation of the proposed computational method was carried out based on comparative analysis of MCNP6.2 predicted and neutron dosimetry measured reaction rates ($^{54}\text{Fe}(n,p)^{54}\text{Mn}$, $^{93}\text{Nb}(n,n')^{93\text{m}}\text{Nb}$, $^{58}\text{Ni}(n,p)^{58}\text{Co}$) on the outer surface of ANPP Unit #2 RPV. Validation revealed that MCNP6.2 predicted fast neutron fluence results are very sensitive to the ENDF-B neutron data. Particularly, MCNP6.2 with ENDF/B-VIII.0 significantly underpredicts (20%-30%) fast neutron fluence while using ENDF/B-VII.1 data overpredicts it. Adding revised beta-released evaluations of Fe-54, Fe-56, Fe-57, O-16 from INDEN to the ENDF/B-VIII.0 allows to get reasonable agreement with measurement results for all types of measured reaction rates.

Keywords: neutron fluence, RPV, validation, WWER

I. INTRODUCTION

One of the critical challenges of the long-term operation of nuclear reactors is the justification of the residual lifetime of non-replaceable safety-significant SSCs. The reactor pressure vessel (RPV) is the crucial component of NPP that determines the feasibility of the long-term operation of the reactor. The fast neutron fluence is one of the most important mechanisms of degradation of the safety features of the RPVs. Therefore, validating the simulation tools used in quantification of neutron fluence to support Regulatory Body decision-making is paramount.

The computational route allows to integrate deterministic 2D lattice and 3D nodal diffusion calculation results as a 3D (pin-wise axially distributed) fixed neutron source and material properties (3D density and temperature distributions) for each time point of fuel cycle in the full-scale Monte Carlo neutron transport model with the most recent continuous energy ENDF/B neutron data libraries. It was developed by taking into account the most recent and stringent requirements [1] as well as valuable insights from past research devoted to LWR fast neutron fluence analysis [2, 3, 4].

One of the three important steps required by [1] for qualification of the neutron transport calculational methodology is validation of it against operating reactor measurements data. The suggested computational route has been validated against following neutron dosimetry measured reaction rates - $^{54}\text{Fe}(n,p)^{54}\text{Mn}$, $^{93}\text{Nb}(n,n')^{93m}\text{Nb}$, $^{58}\text{Ni}(n,p)^{58}\text{Co}$ on the outer surface of ANPP Unit #2 RPV[5]. Measured specific activities of neutron dosimeters allow not only to quantify fluence neutrons having energies greater 1 MeV but also have detailed spectral picture of neutron fluence.

Developed HELIOS/BIPR/PARCS/MCNP6 RPV fast neutron fluence computational route validation results are presented in this paper.

II. DESCRIPTION OF THE MEASUREMENTS [5]

Neutron detectors were attached to the irradiation frame that was installed on the outer surface of the ANPP Unit 2 RPV. It consists of (see Fig. 1) central vertical rod with neutron dosimeters, fixed on the outer surface of the reactor pressure vessel with the help of cables; 3 arc-shaped holders of neutron dosimeters, placed so that the upper and lower arcs of the holders are at the level of the 4th and 5th welds of RPV, and the central arc of the holder is at the level of the reactor core center; left and right vertical cables (stretched between the edges of the upper and lower arcs), on which the neutron dosimeters are fixed with the help of special clamps.

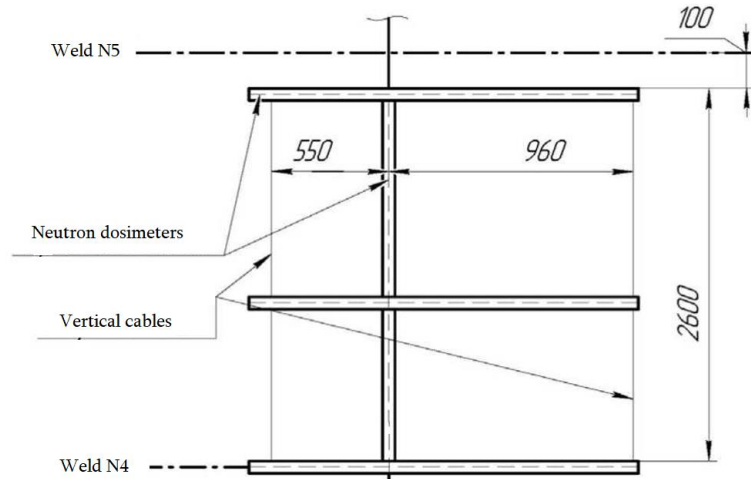


Figure 1. General layout of the irradiation frame on the outer surface of the reactor vessel

Horizontal neutron dosimeters' holders cover 45 degrees of the circumference of the reactor pressure vessel. Each set of dosimeters installed on the irradiation structure included neutron activation detector made of Fe (with enrichment of the isotope ^{54}Fe 99.77 wt.%) and Nb (tantalum impurity content not more than 3 ppm). In separate positions Ni detectors with a purity of at least 99.9 % were installed additionally.

Neutron dosimeters were irradiated for 300 calendar days (214 effective days). Power change during the 30th fuel cycle is shown in the Fig. 2. Power history of fuel cycle was used for the correct determination of specific activities of ^{54}Mn , ^{58}Co , and $^{93\text{m}}\text{Nb}$ isotopes in dosimeters.

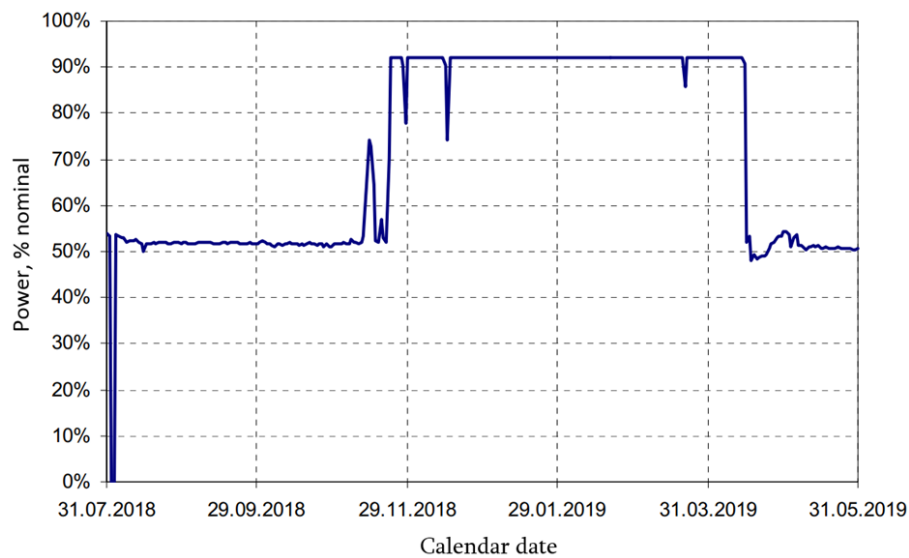


Figure 2. Time evolution of ANPP reactor core power during 30th fuel cycle

Measurements of the absolute activities of the iron, nickel dosimeters were carried out in accordance with [6,7] standards.

III. NEUTRON SOURCE CALCULATION

Nodal neutron source $S(i, j, k, t, E)$ (number of neutrons emitted per second by k -th axial node of j -th fuel rod belonging to the i -th fuel assembly at time point t was calculated with the following formula:

$$S(i, j, k, t, E) = \alpha \cdot P(i, j, k, t) \frac{v(i, j, k, Bu)}{Q(i, j, k, Bu)} Chi(Bu, E),$$

$$Chi(Bu, E) = \sum_i \sum_j \sum_k chi(i, j, k, Bu, E) / (i * j * k),$$

where $P(i, j, k, t)$ is the power of k -th axial node of j -th fuel rod belonging to the i -th fuel assembly at time point t ; $v(i, j, k, Bu)$ and $Q(i, j, k, Bu)$ are number of neutrons per fission emitted in and energy released per fission in k -th axial node of j -th fuel rod belonging to the i -th fuel assembly having burnup Bu ; $chi(i, j, k, Bu, E)$ is fission spectra of k -th axial node of j -th fuel rod belonging to the i -th fuel assembly having burnup Bu ; $\alpha = 6.2415 \cdot 10^{18}$ is a constant reflecting conversion of fission energy from MeV to Joule. Averaging of the neutron spectra was carried out over 4 fuel assemblies placed in outermost radial positions (see Fig. 3). $v(Bu)$, $Q(Bu)$ and $chi(Bu, E)$ values were calculated by HELIOS-2 program [8] using following formalism

$$v(Bu) = \frac{\sum_i v_i \Sigma_f^i \Phi_i}{\sum_i \Sigma_f^i \Phi_i}, \quad Q(Bu) = \frac{\sum_i Q_i \Sigma_f^i \Phi_i}{\sum_i \Sigma_f^i \Phi_i}.$$

where summation is going through all fissionable isotopes.

Burnup dependent neutron $chi(Bu, E)$ spectra energy group structure was setup in the HELIOS-2 model to correspond to the energy bins of BUGLE-96 cross section library [9].

The Source module of Fluence program was developed by Python that reads pin-wise axial power and burnup distributions from ANPP BIPR-7A [10] nodal diffusion code output file, $v(Bu)$ and $Q(Bu)$ burnup dependent vectors from HELIOS-2 output. Then based on the 3D burnup distribution it assigns $v(i, j, k, Bu)$, $Q(i, j, k, Bu)$ values, $chi(i, j, k, Bu, E)$ spectra and makes polynomial interpolations as necessary for burnup values that are within burnup steps used in HELIOS-2 model. In the final step, the Source module based on read and assigned/interpolated values prepares a fixed neutron source compatible with MCNP6.2 [11] SDEF lattice source format with cell rejection technique.

As can be seen on Fig. 2, there are significant changes in the power over time during simulated fuel cycle that are essential for both amplitude of neutron source and spectral changes due to water density changes and burnup increment. For getting sufficiently accurate neutron source 30th fuel cycle duration was subdivided in 15 time steps in a way that time step is 3.5 times smaller than the half-life of the shortest living reaction product (⁵⁸Co).

IV. MCNP6.2 MODEL OF WWER-440

The MCNP 6.2 WWER-440 reactor model covers reactor core, core baffle, core barrel, downcomer, RPV cladding, RPV, thermal insulation and dry shielding (see Fig. 3 and Fig. 4). In the reactor core part of the model geometry, materials and the neutron source were modeled in pin-by-pin level. The initial full core model was azimuthally and radially truncated via assignment of importance values to sample only those assemblies that effectively contribute to the detector response. Azimuthal truncation was determined by neutron activation detectors' spatial positioning. Remained core model covers 120-degree segment of the core WWER-440 core including neighboring 60-degree rotational symmetry portions.

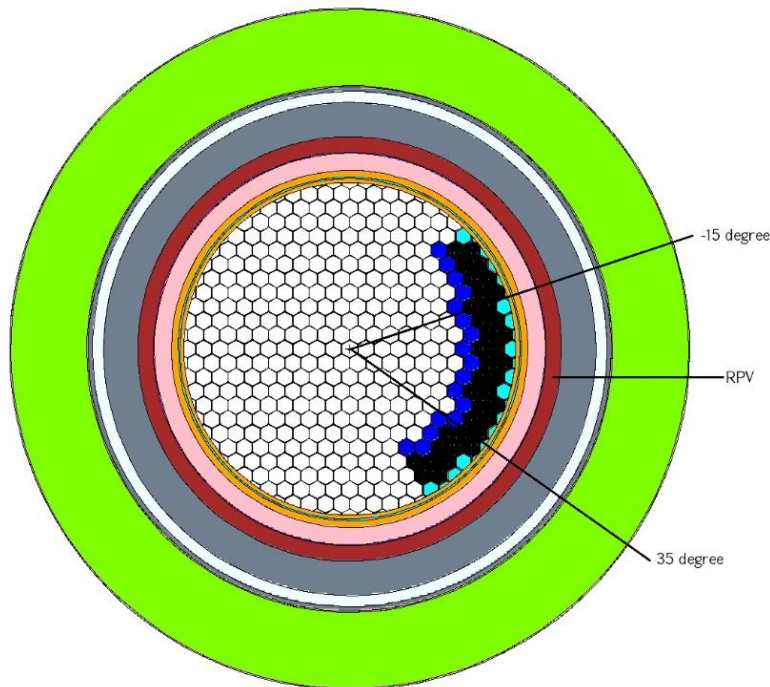


Figure 3. R- θ cross-section of the reactor model at half-height of the core

Model radial truncation is based on sensitivity analysis of the neutron fluence. Experience suggests [3] that neutrons sampled from the central part of the core don't

significantly contribute to the fluence of neutrons on the outer surface of RPV. By sensitivity analysis of the developed core model, it was concluded that the model containing fuel assemblies at least in the 2 outermost hexagonal rows for each azimuthal direction is sufficiently accurate and computationally affordable.

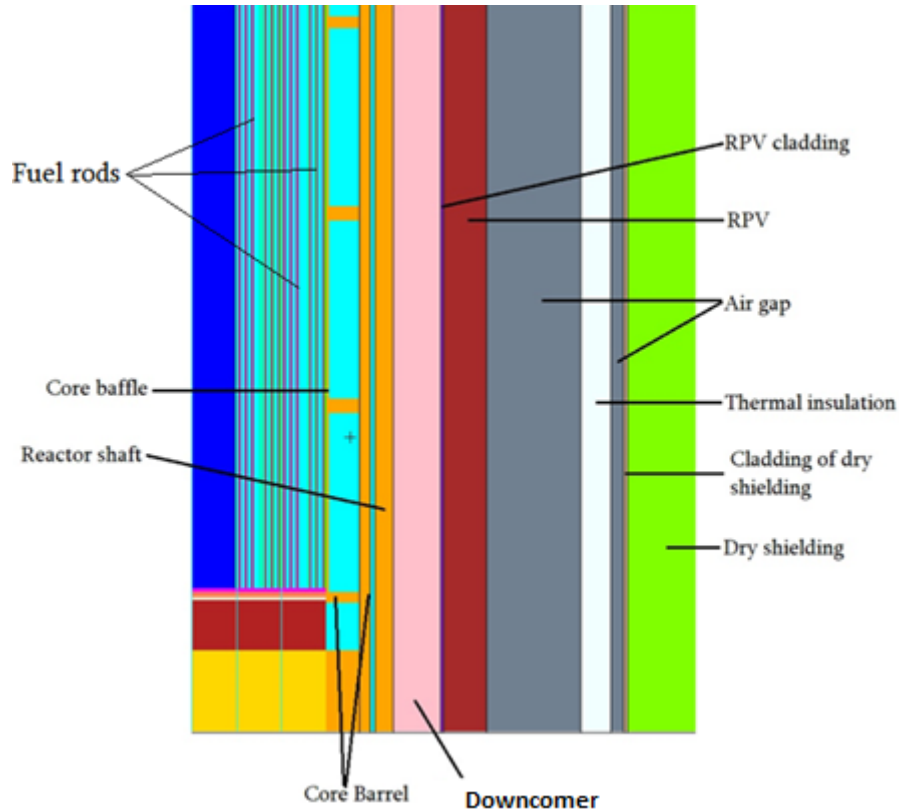


Figure. 4 R-Z cross-section of the reactor model at 0 azimuthal angle

Since fast neutron fluence is sensitive to the water density both in terms of moderation and leakage, the following axial nodalization was applied:

- in the core part fuel rod and surrounding water were subdivided into the 43 axial nodes: 41 equidistant axial nodes covering fuel part (corresponding to the PARCS-PATHS model axial nodalization), 1 node for each of tail and header parts of fuel assembly;
- bypass water after core baffle is subdivided into the 10 axial nodes since in this region water temperature gradient is less pronounced.

To calculate regional number densities/temperatures of relevant materials to be used in MCNP 6.2 model, neutronics analysis of the 30th fuel cycle of ANPP was carried out by PARCS-PATHS code. ANPP model for cycle analysis developed by PARCS-PATHS was verified and

validated based on ANPP operational data. As fast neutron fluence is the most sensitive to the density of water in downcomer, time discretization for the 30th fuel cycle was synchronized with the fluence calculation time intervals, to properly catch water density changes in the downcomer due to power changes (see Fig. 2). The density module of the Fluence program was developed to extract regional number densities/temperatures of relevant materials and use them in the MCNP 6.2 model.

Cross-section for each dosimeter nucleus taken from International Reactor Dosimetry and Fusion File (IRDF-II) [12].

V. ANALYSIS OF THE RESULTS

Initial validation calculations were carried out with latest ENDF/B-VIII.0 [13] continuous cross-sections library available at the time of simulations. However, results of analysis showed significant under-prediction of ^{93m}Nb isotope (see Fig. 5), therefore neutrons having energies above 1MeV. Discussions with NDC at BNL showed that during release of ENDF/B-VIII.0, iron spheres neutron leakage measurement data [14] were not taken into account during ENDF/B-VIII.0 evaluation. Furthermore, paper [15] identified essential difference on the neutron fluence calculations for WWER-1000 reactors. Sensitivity analysis of our calculations for WWER-440 reactor with using ENDF/B-VII.1 and ENDF/B-VIII.0 confirmed conclusions of that neutrons's inelastic scattering on iron and elastic scattering on oxygen are mainly responsible for observed fluence differences, with predominant role of iron isotopes, particularly Fe-56. Currently, beta-released evaluations of Fe-54, Fe-56, Fe-57, O-16 are available in INDEN at IAEA website [16]. So, in this work results of fluence analysis with ENDF/B-VII.1, ENDF/B-VIII.0 and ENDF/B-VIII.0 amended with beta-released Fe-54, Fe-56, Fe-57, O-16 isotopes cross-sections (further in the text we will refer it as ENDF/B-VIII.0+) are discussed. In the Figures 5 and 6 azimuthal distributions of predicted and measured activities of ^{54}Mn , ^{58}Co and ^{93m}Nb at 13cm and 107cm from bottom of the reactor core are shown. The 13cm axial position is very important for WWER-440 reactors since its corresponds to the position of the axial circumferential weld of the RPV. Results of comparative analysis show that using amended ENDF/B-VIII.0+ library brings very good agreement between measured and predicted specific activities of ^{54}Mn and ^{58}Co at 13cm (respective average C/M values are 0.98 and 1.01). It improves agreement with measured ^{93m}Nb , however under-prediction is still observed even with using of ENDF/B-VII.1 library [17] (average C/M=0.83). ENDF/B-VIII.0 results are out of $\pm 20\%$ band from measured values.

At 107cm agreement with predicted and measured ^{93m}Nb activities is significantly improved (average C/M=0.95) by applying ENDF/B-VIII.0+ library. For ^{54}Mn , ^{58}Co over-prediction is observed with respective 1.13 and 1.15 average C/M values.

In the Fig. 7 axial distributions of the activities of ^{54}Mn , ^{58}Co , ^{93m}Nb at -11.7 degree azimuthal angle are presented. As we can see, use of the amended ENDF/B-VIII.0+ library produces reasonable agreement for all isotopes activities (average C/M values for ^{54}Mn , ^{58}Co , ^{93m}Nb are 1.11, 1.14 and 0.92) while with ENDF/B-VII.1 and ENDF/B-VIII.0 libraries marginal results are obtained for certain isotopes.

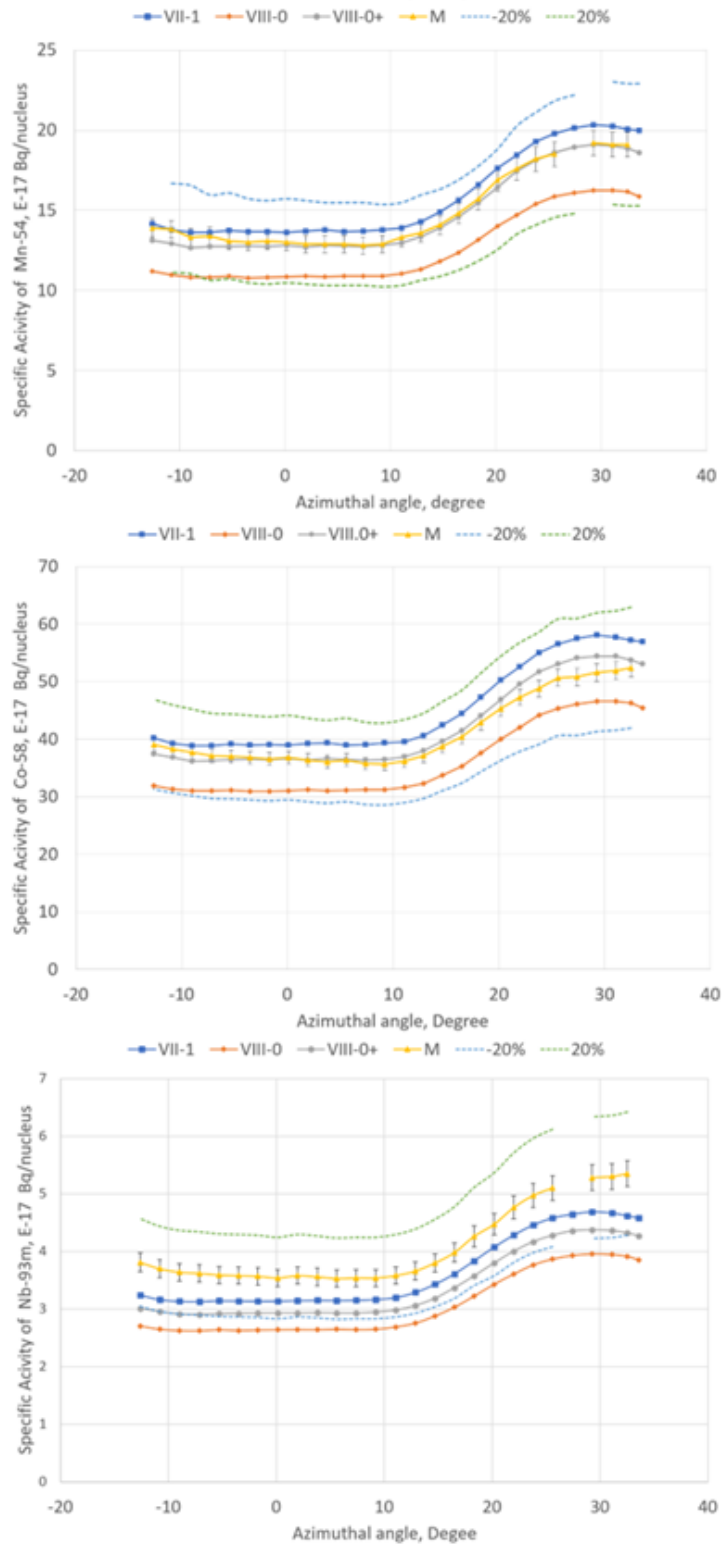


Figure. 5 Azimuthal distributions of predicted and measured activities of ^{54}Mn , ^{58}Co , $^{93\text{m}}\text{Nb}$ at 13cm

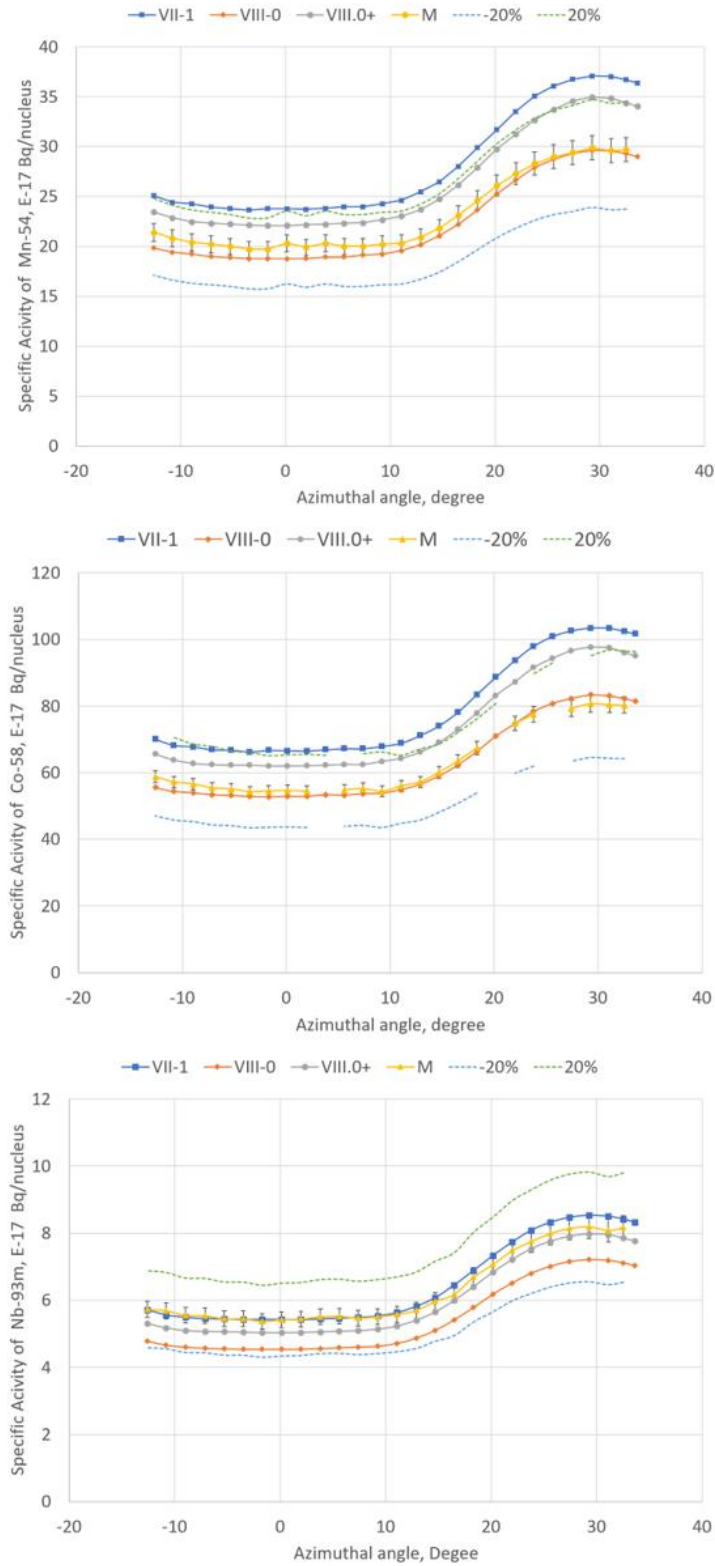


Figure. 6 Azimuthal distributions of predicted and measured activities of ^{54}Mn , ^{58}Co , $^{93\text{m}}\text{Nb}$ at 107cm

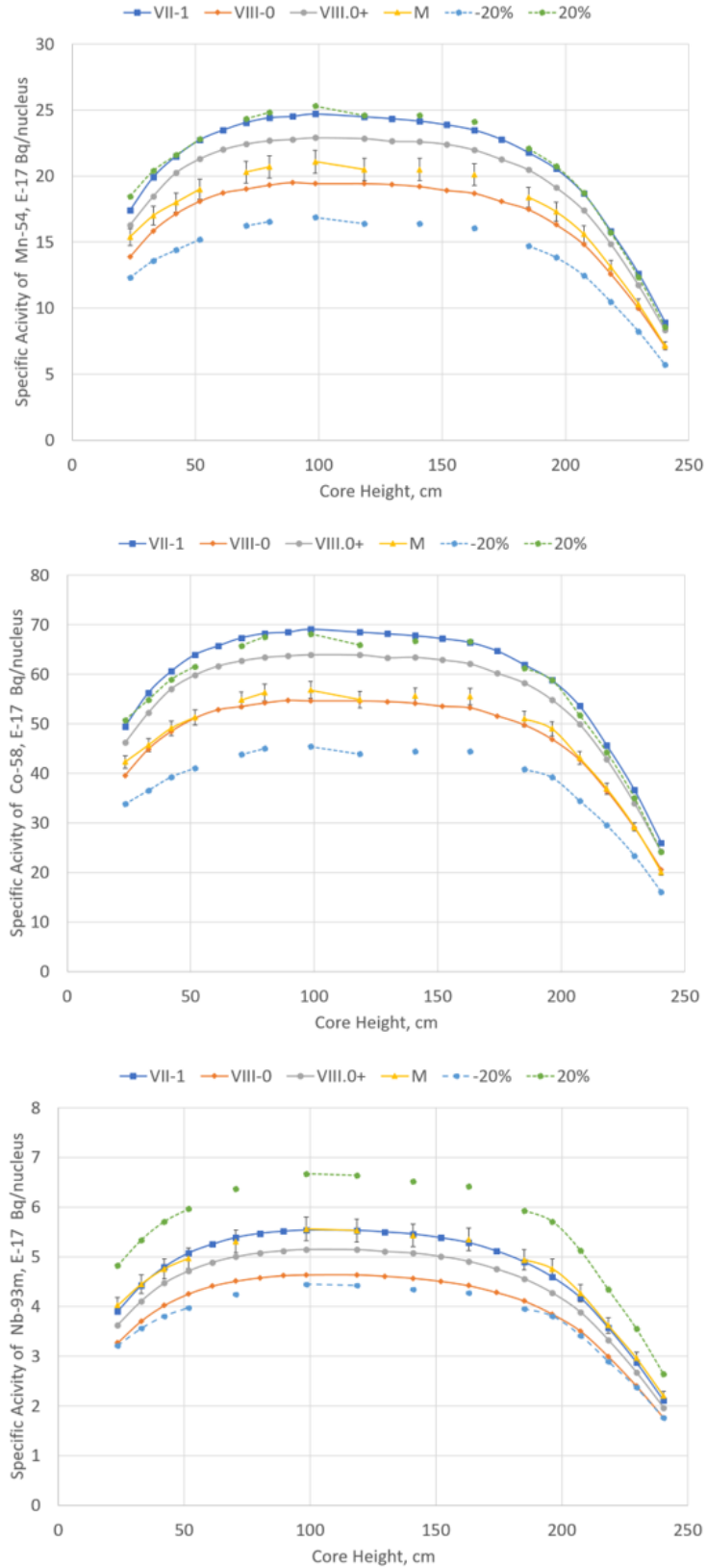


Figure. 7 Axial distributions of predicted and measured activities of ^{54}Mn , ^{58}Co , $^{93\text{m}}\text{Nb}$ at -11.70

VI. CONCLUSIONS

Validation of HELIOS/BIPR/PARCS/MCNP computation route for WWER-440 reactor pressure vessel neutron fluence analysis was performed. Results of these analyses indicate that neutron fluence is very sensitive to the neutron cross-sections libraries. Particularly, generally use of ENDF/B-VII.1 library overpredicts while ENDF/B-VIII.0 underpredicts fluence values with regard of the measurements. Use of amended ENDF/B-VIII.0 cross-sections library with beta-released Fe-54, Fe-56, Fe-57, O-16 isotopes cross-sections allows to get reasonable agreement for all energy neutrons above 1 Mev.

REFERENCES

1. Calculational and Dosimetry Methods for Determining Pressure Vessel Neutron Fluence, Regulatory Guide 1.190 (2001)
2. A. HAGHIGHAT, M. MAHGEREFTEH, B. PETROVIC, "Evaluation of the Uncertainties in the Source Distribution for Pressure Vessel Neutron Fluence Calculations", Nuclear Technology, 109:1, 54-75, (1995).
3. A. VASILIEV, H. FERROUKHI, et al, "Development of a CASMO-4/SIMULATE-3/MCNPX calculation scheme for PWR fast neutron fluence analysis and validation against RPV scraping test data", Annals of Nuclear Energy 34, 615–627 (2007).
4. M. TODOSOW, J. CAREW, P. KOHUT, "Evaluation of selected approximations used in pressure vessel calculations", Trans. Am. Nucl. Soc. 46, 658–659 (1984).
5. " Measurement of the Activities of Neutron Activation Indicators Irradiated on the Outer Surface of the Reactor Pressure Vessel of Unit 2 of ANPP", Report of Kurchatov Institute, 109.1-71BH (2019).
6. ASTM E 263-18. Standard Test Method for Measuring Fast-Neutron Reaction Rates by Radioactivation of Iron (2013)
7. ASTM E 264-19. Standard Test Method for Measuring Fast-Neutron Reaction Rates by Radioactivation of Nickel (2013).
8. C. WEMPLE, H. GHEORGHIU, R. STAMMLER, E. VILLARINO, The HELIOS-2 Lattice Physics Code, International Conference on the Physics of Reactors, Interlaken, Switzerland, 1-14 (2008)

9. J. WHITE, D. INGERSOLL, C. SLATER, R. ROUSSIN, “BUGLE-96: A revised multigroup cross section library for LWR applications based on ENDF/B-VI Release 3”, CONF-960415-37 (1996)
10. BIPR-7A (version 1.5), Attestation passport N 613 (2006).
11. J. T. GOORLEY, F. B. BROWN, et al, “MCNP6TM User’s Manual” (2013)
12. A. Trkov, P.J. Griffin at all, IRDFF-II: A New Neutron Metrology Library. Special Issue of Nuclear Data Sheets, Vol. 163, pp. 1-108 (2020)
13. D. BROWN, M.B. CHADWICK, R. CAPOTE, et all “ENDF/B-VIII.0: The Major Release of the Nuclear Reaction Data Library with CIELO-project Cross-Sections, New Standards and Thermal Scattering Data”, Nuclear Data Sheets, 148, 1-142 (2018)
14. E. Sajo, M. Williams, M. Asgari, “Comparison of measured and calculated neutron transmission through steel for a ²⁵²Cf source”, Annals of Nuclear Energy 20 (1993)
15. M. LOVECKY, K. GINCELOVÁ, P. HAROKOVÁ, “Performance of ENDF/B-VIII.0 library for VVER reactors criticality safety, fuel depletion and reactor dosimetry applications”, Annals of Nuclear Energy 148 (2020)
16. <https://www-nds.iaea.org/INDEN/>
17. M.B. CHADWICK, M. HERMAN, P. OBLOŽINSKÝ, et all “ENDF/B-VII.1 Nuclear Data for Science and Technology: Cross Sections, Covariances, Fission Product Yields and Decay Data”, Nuclear Data Sheets, 112, 2887 (2011)